$K^h\alpha_{1,2}$ X-Ray Hypersatellite Line Broadening as a Signature of K-Shell Double Photoionization Followed by Outer-Shell Ionization and Excitation

M. Polasik,[1,*] K. Słabkowska,[1] J. Rzadkiewicz,[2,3] K. Kozioł,[1] J. Starosta,[1] E. Wiatrowska-Kozioł,[1] J.-Cl. Dousse,[4] and J. Hoszowska[4]

[1]*Faculty of Chemistry, Nicholas Copernicus University, 87-100 Toruń, Poland*
[2]*Soltan Institute for Nuclear Studies, 05-400 Otwock-Świerk, Poland*
[3]*Institute of Plasma Physics and Laser Microfusion, Hery 23, 01-497 Warsaw, Poland*
[4]*Physics Department, University of Fribourg, CH-1700 Fribourg, Switzerland*

We propose a novel approach for the theoretical analysis of the photoinduced high-resolution $K^h\alpha_{1,2}$ x-ray hypersatellite spectra, which allows us to obtain reliable values of lifetimes of the doubly K-shell ionized states and fundamental information about the relative role of K-shell double photoionization (DPI) mechanisms. It is demonstrated for the first time that the $K^h\alpha_{1,2}$ hypersatellite natural line broadening observed for selected metal atoms with $20 \leq Z \leq 30$ can be well reproduced quantitatively by taking into account the influences of the open-shell valence configuration (adopted from predictions of the band-structure method) and the outer-shell ionization and excitation following the DPI process.

Observed for the first time by Charpak [1] and enlightened by Briand *et al.* [2], the $K^h\alpha_{1,2}$ x-ray hypersatellite lines originate from the $1s^{-2} \rightarrow 1s^{-1}2p^{-1}$ transitions (i.e., from the radiative decay of initial K^{-2} states with two holes in the K shell). Thanks to the development of intense energy-tunable x-ray synchrotron radiation sources, the observation of photoinduced high-resolution $K^h\alpha_{1,2}$ hypersatellite spectra has become feasible [3–8]. From the interpretation of these hypersatellite spectra, rich and valuable information can then be obtained about the properties of K-shell hollow atoms (i.e., atoms with an empty K shell and occupied outer shells) as well as about the double photoionization (DPI) mechanisms.

At present, it is well established [3–7,9] that the absorption of a single photon can lead to K-shell DPI via two different mechanisms: (i) a purely quantum mechanical shakeoff (SO) and (ii) a (quasi)classical knockout (KO). In the SO mechanism leading to DPI, the primary K-shell photoelectron is ejected rapidly, and due to the sudden change of the atomic potential the second K-shell electron is ionized. In the KO process the outgoing first K-shell photoelectron knocks out the second K-shell electron. Very recently high-resolution measurements of $K^h\alpha_{1,2}$ hypersatellite x-ray spectra induced by photoionization were reported by Hoszowska *et al.* [3,4] for several light elements with $12 \leq Z \leq 23$. From these measurements the photon energy dependence of the K-shell DPI was determined and a semiempirical model to separate both DPI mechanisms was proposed. In that work it was concluded that near threshold and at intermediate photon energies the K-shell DPI is dominated by the KO mechanism, the SO mechanism being important only at high photon energies. These findings support the conclusions of Kanter *et al.* [6] and Huotari *et al.* [7] for medium-Z atoms.

The theoretical evaluation of the $K^h\alpha_{1,2}$ natural linewidths is based on the following formula:

$$\Gamma_{K^h\alpha_{1,2}} = \Gamma_{KK} + \Gamma_{KL_{3,2}}, \tag{1}$$

where Γ_{KK} and $\Gamma_{KL_{3,2}}$ are the natural widths of the doubly ionized K^{-2} and $K^{-1}L_{3,2}^{-1}$ states which correspond to the initial and final states of the $K^h\alpha_{1,2}$ hypersatellite transitions, respectively. The width of the $K^{-1}L_{3,2}^{-1}$ state can be approximated by

$$\Gamma_{KL_{2,3}} \simeq \Gamma_K + \Gamma_{L_{3,2}}, \tag{2}$$

where Γ_K and $\Gamma_{L_{3,2}}$ are the natural widths of the singly ionized K^{-1} and $L_{3,2}^{-1}$ states, respectively. The first empirical estimation of the $K^h\alpha_{1,2}$ natural linewidths was proposed by Mossé *et al.* [10] who employed Eq. (1), assuming for the width of the K^{-2} state the following approximation $\Gamma_{KK} = 2\Gamma_K$. However, it was found later that the $K^h\alpha_{1,2}$ linewidths derived from high-resolution K-hypersatellite spectra induced by DPI [5,8] were systematically bigger than those obtained using Mossé's approximation. The modifications of Eq. (1) for the LS and intermediate coupling regime (low- and medium-Z regions) proposed by Rzadkiewicz *et al.* [11] lead to even higher disagreement between theory and experiment. The changes in the fluorescence yields considered by Chen [12] were found to be relatively small and did not allow one to eliminate the observed discrepancies. All these considerations lead to the conclusion drawn by Diamant *et al.* [8] that no good physical reason could be found to explain the observed $K^h\alpha_{1,2}$ line broadenings nor the resulting reduced lifetimes of the K^{-2} states.

In this Letter we propose a novel approach for the theoretical analysis of the photoinduced high-resolution

$K^h\alpha_{1,2}$ x-ray hypersatellite spectra measured for thin solid targets. This approach permits us to explain the broadening of the hypersatellite lines and allows us to obtain information about the relative importance of the different K-shell DPI mechanisms.

First, we determined the radiative natural widths of the K^{-2} states, using multiconfiguration Dirac-Fock (MCDF) calculations including the transverse (Breit) interaction and QED corrections (see, e.g., [13] and references therein). The total natural widths Γ_{KK} and the mean lifetimes of K^{-2} states τ_{KK} were then computed from the following simple relations:

$$\Gamma_{KK} = \Gamma_{KK}^{\mathrm{rad}} + \Gamma_{KK}^{\mathrm{nonrad}}, \tag{3}$$

$$\tau_{KK} = \frac{\hbar}{\Gamma_{KK}}, \tag{4}$$

where $\Gamma_{KK}^{\mathrm{rad}}$ are the radiative natural widths and $\Gamma_{KK}^{\mathrm{nonrad}}$ the nonradiative natural widths. For the nonradiative widths the values of Chen [12] adopted directly for Cr and Zn and interpolated for Ca, V, and Co, with ~1% accuracy, were employed. The $K^h\alpha_2$ and $K^h\alpha_1$ natural linewidths were evaluated on the basis of the calculated [according to Eq. (3)] total natural widths of the K^{-2} states and the total widths of the K^{-1}, L_2^{-1}, and L_3^{-1} states tabulated by Campbell and Papp [14].

Our theoretical predictions for the total natural widths of the K^{-2} level and the $K^h\alpha_2$ and $K^h\alpha_1$ natural linewidths for selected atoms with $20 \leq Z \leq 30$ are presented in Table I. The calculated mean lifetimes of the K^{-2} doubly ionized states are also listed (last column). For all elements it is found that the latter are about 2.2 times shorter than those of the K^{-1} singly ionized states. The comparison of the theoretical linewidths derived from Eq. (1) with the available experimental $K^h\alpha_2$ and $K^h\alpha_1$ values obtained from photoinduced x-ray spectra [4,8] shows that our ''basic procedure'' results (columns 4 and 9 in Table I) are much smaller than the experimental values, the deviations being particularly pronounced for the open outer-shell elements.

One of the reasons for the observed differences is the so-called open-shell valence configuration (OVC) effect. The latter is related to the fact that, in the case of open-shell atoms, there are for each transition many initial and final states. A transition consists then of numerous overlapping components having slightly different energies and widths. As a consequence of the OVC effect, the effective natural $K^h\alpha_{1,2}$ linewidths are much larger than those predicted by Eq. (1). In view of the fact that in the solid state the valence configurations are different from those of free atoms, we have adopted in our evaluation of the OVC effect valence shell configurations that are as close as possible to the ones predicted by the augmented plane-wave band-structure calculations, i.e., $3d^{3.98}4s^{1.02}$, $3d^{4.96}4s^{1.04}$, and $3d^{7.87}4s^{1.13}$ for V, Cr, and Co, respectively [15,16]. We have also checked that the modifications of the valence configurations for Ca and Zn do not noticeably influence the widths of the $K^h\alpha_{1,2}$ lines (differences were found to be less than 0.02 eV). Therefore, for Ca and Zn, we present results for closed-shell configurations.

In order to evaluate the influence of the OVC effect on the $K^h\alpha_{1,2}$ natural linewidths, we have synthesized the hypersatellite spectra using the ''basic'' natural linewidth data quoted in Table I (columns 4 and 9). Results of this evaluation procedure are illustrated for the open-shell Co atom in Fig. 1. For both hypersatellite transitions the theoretical stick spectra (MCDF component energies with their relative intensities—red sticks in Fig. 1) and the synthesized spectra corresponding to the sums of the overlapping Lorentzians attached to each MCDF component (red dashed line in Fig. 1) are depicted. The synthesized spectra were then fitted using one Lorentz profile for the $K^h\alpha_2$ line and one for the $K^h\alpha_1$ line (blue solid lines in Fig. 1). In order to evaluate the broadening arising from the OVC effect, the widths of these fitted Lorentzians were compared to the widths determined from Eq. (1) (the corresponding Lorentzians are

TABLE I. Theoretical MCDF-based predictions for the total widths and lifetimes of the K^{-2} states, the evaluated natural linewidths of the $K^h\alpha_2$ and $K^h\alpha_1$ lines for selected metal atoms with $20 \leq Z \leq 30$, and the available experimental linewidths. Numbers in parentheses are the uncertainties in the last digits of the numbers cited.

Atom	Configuration	Width of K^{-2} state (eV)	Natural linewidths (eV)										Lifetime of K^{-2} state (10^{-16} s)
			$K^h\alpha_2$					$K^h\alpha_1$					
			Eq. (1)	OVC[a]	OIE1[b]	OIE2[c]	Exp.	Eq. (1)	OVC[a]	OIE1[b]	OIE2[c]	Exp.	
$_{20}$Ca	$(4s^2)$	1.87	2.85	2.85	2.99	3.63	3.72(18)[d]	2.85	···	···	···	···	3.52
$_{23}$V	$(3d^4 4s^1)$	2.24	3.53	5.20	5.28	5.46	5.5(1)[e] 5.54(19)[d]	3.53	5.35	5.47	5.66	6.0(6)[e] 5.6(10)[d]	2.94
$_{24}$Cr	$(3d^5 4s^1)$	2.39	3.73	5.41	5.59	5.77	5.7(1) [e]	3.73	6.60	6.72	6.90	5.0(9) [e]	2.75
$_{27}$Co	$(3d^8 4s^1)$	2.96	4.66	5.82	6.17	6.80	6.7(1) [e]	4.67	6.19	6.52	6.94	7.1(6) [e]	2.24
$_{30}$Zn	$(3d^{10} 4s^2)$	3.69	5.92	5.92	6.49	7.23	7.5(4) [e]	5.93	5.93	6.06	6.59	6.4(7) [e]	1.78

[a]Effective linewidths including only the OVC effect. [b]Effective linewidths with the OIE1 and OVC broadenings.
[c]Effective linewidths with the OIE2 and OVC broadenings. [d]Hoszowska *et al.* [4]. [e]Diamant *et al.* [8].

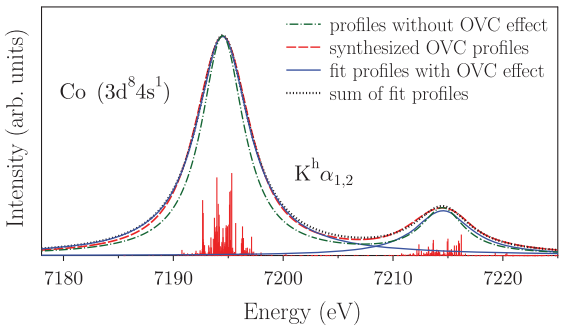

FIG. 1 (color online). The OVC effect evaluation of the effective $K^h\alpha_{1,2}$ natural linewidth for the open-shell Co atom.

represented by the green dash-dotted line in Fig. 1). As shown, the profiles including the OVC effect are significantly broader than those without the OVC effect. This procedure which was performed for all open-shell elements permits us to diminish substantially the differences between the theoretical and experimental results (see "OVC" and "Exp." columns in Table I).

Another reason for the significant broadening observed experimentally for the $K^h\alpha_{1,2}$ x-ray lines can be attributed (for all elements) to the outer-shell ionization and excitation (OIE) effect. In order to evaluate the OIE broadening we have performed calculations of the total shake probabilities, i.e., SO and shakeup (SU), applying the sudden approximation (SA) model [17] and using MCDF wave functions [13]. Three theoretical scenarios were considered. In the first one (OIE1), the fast single K-shell ionization is followed by shake processes that remove the second $1s$ electron and some valence electrons. As the shaken $1s$ electron is slow, the valence electron is assumed to be affected only by the sudden atomic potential change resulting from the removal of the fast $1s$ photoelectron. In the second scenario (OIE2), the outer-shell shake process is due to the K-shell double ionization, assuming that the two $1s$ electrons are removed quasisimultaneously and escape both at high enough velocities. In the OIE2 case the potential change is more pronounced and thus the shake probability bigger. In the third scenario shake processes are energetically forbidden so that no OIE broadening is expected. The subshell shake probabilities calculated for the OIE1 and OIE2 scenarios are presented in Table II. As shown, the OIE2 total shake probabilities are a few times bigger than the OIE1 ones.

The evaluation procedure of the OIE effect (OIE2 scenario) for the case of the $K^h\alpha_2$ transition of the closed-shell Ca atom is illustrated in Fig. 2. Shown are the hypersatellite transition (blue long-dashed line), the hypersatellite satellites corresponding to $3p$, $4s$, and $3p4s$ spectator holes produced by the OIE effect, and the sum of all lines (red solid line). The Lorentzian corresponding to the fit of the sum is also depicted (black dash-dot-dot line). The latter was used to determine the effective linewidth of the

TABLE II. Total shake probabilities (in percent per subshell) as a result of double K-shell ionization (the OIE2 scenario) for selected atoms (calculated for the same valence configurations as presented in Table I). Numbers in parentheses are the values for single K-shell ionization (the OIE1 scenario).

	Probabilities per subshell (%)					
Atom	$2s$	$2p$	$3s$	$3p$	$3d$	$4s$
$_{20}$Ca	0.75	4.12	3.81	36.14		49.03
	(0.21)	(1.26)	(1.31)	(10.74)		(20.23)
$_{23}$V	0.59	3.06	2.97	18.96	47.82	25.50
	(0.16)	(0.89)	(0.78)	(4.89)	(18.25)	(9.35)
$_{24}$Cr	0.54	2.77	2.59	16.48	47.76	24.74
	(0.15)	(0.80)	(0.68)	(4.22)	(18.29)	(9.18)
$_{27}$Co	0.42	2.11	1.82	11.44	45.99	23.24
	(0.11)	(0.59)	(0.47)	(2.89)	(15.25)	(8.88)
$_{30}$Zn	0.32	1.65	1.23	9.16	34.49	31.07
	(0.09)	(0.46)	(0.34)	(2.34)	(10.45)	(11.70)

hypersatellite transition. As can be seen, the distinct contributions of the satellite groups of the hypersatellite (which are shifted with respect to the "pure" hypersatellite) result in an increase of the effective $K^h a_2$ hypersatellite linewidth. On the other hand, the effective line shape of the hypersatellite is very similar for satellites resulting from SO and SU processes (see also Ref. [18]). In the case of open-shell atoms the procedure for the evaluation of the OIE effect includes at the same time the OVC effect. A similar analysis was performed for the other elements and for the OIE1 case (see "OIE2" and "OIE1" columns of Table I).

As can be seen in Table I, the large discrepancies between the experimental data and the linewidths evaluated taking into account only the OVC effect indicate that the third scenario is unlikely. We assign the third scenario (no shake) to DPI via a slow KO mechanism, which can only occur in the very narrow near DPI threshold energy range. The discrepancies between the experimental data and the $K^h\alpha_{1,2}$ linewidth predictions including the OIE1 and the OVC effects ("OIE1" columns in Table I) are only slightly smaller. This indicates that the OIE1 scenario plays only a minor role in the observed linewidth broadening. We assign this scenario to the double K-shell ionization via a $1s$ SO process. This mechanism is predominant at high photon energies [3,4] because, due to the very fast $1s$ photoelectron, shake processes may occur not only in the outer shells but also in the K shell.

For all considered elements there is a good agreement between the experimental data and the effective $K^h\alpha_{1,2}$ linewidths in the case of OIE2 broadening ("OIE2" columns in Table I). This agreement indicates that the OIE2 scenario (with a "strong" shake process) is dominant in the production of the multivacancy states whose deexcitation leads to the analyzed hypersatellite spectra. Note that the experimental linewidths were obtained from hypersatellite spectra measurements performed at photon energies where

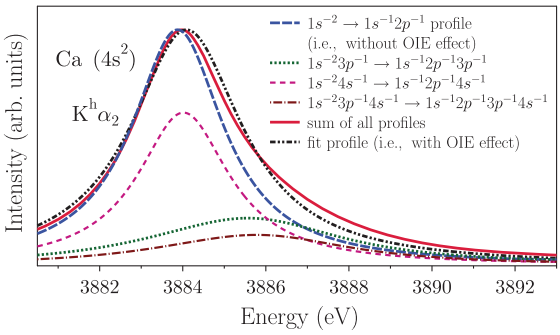

FIG. 2 (color online). Evaluation of the OIE2 broadening in the case of the $K^h\alpha_2$ hypersatellite transition of Ca.

the KO mechanism is dominant, i.e., in the wide energy range around the maximum of the DPI cross section [4] or significantly above threshold for K-shell DPI [8]. Further, it was reported that the KO process proceeds very fast ($\sim 10^{-18}$ s) [9] and for this process the energy sharing between the first and second electron is nearly symmetric [19,20]. Therefore, the "billiardlike" production of the second K-shell hole should be sudden enough in the time scale of the outer shell to treat the ejection or excitation of outer-shell electrons (via SO and SU processes) in the SA model. We assign thus the OIE2 scenario to the ionization and excitation processes following the K-shell DPI via a fast KO mechanism.

It is worth underlining that the completely different nature of the K-shell DPI via the SO and via the KO mechanisms [19,20] implicates that the strong (OIE2) shake process should be excluded in the SO case. Moreover, in the SO mechanism the shaken K-shell electron seems to be too slow [19,20] to make a sudden potential change, even for an outer-shell electron and the possibility of broadening as a result of the shake cascade seems to be negligible. It is worth noting that there is a lack of experimental data for the $K^h\alpha_{1,2}$ linewidths in the very high photon energy range. Our theoretical predictions for the OIE1 case can be treated as a lower limit for linewidths measured at high photon energies because contributions of the fast KO and other processes cannot be neglected. Since the magnitude of the linewidth broadening depends on the K-shell DPI mechanism followed by OIE processes, the experimental values of $K^h\alpha_{1,2}$ linewidths can be used to probe the relative role of the K-shell DPI mechanisms.

In conclusion, we propose a novel approach for the theoretical analysis of high-resolution $K^h\alpha_{1,2}$ x-ray hypersatellite spectra induced by photons at different energies. For the first time, predictions for the effective natural $K^h\alpha_{1,2}$ linewidths taking into account the OVC effect (including predictions of the band-structure method) and the OIE effect (based on shake probability calculations) allowed us to reproduce quantitatively the $K^h\alpha_{1,2}$ linewidths observed in experiments using thin solid targets. Since the OIE effect is specific to KO and SO processes, from the measured linewidths' analysis it was possible to obtain fundamental information about the relative role of the K-shell DPI mechanisms. On the basis of a detailed theoretical analysis it was found that, in the considered cases, the fast KO process plays a dominant role in the K-shell DPI, as indicated by the large broadening of the observed $K^h\alpha_{1,2}$ lines. This finding confirms the conclusions of Hoszowska *et al.* [3,4], Huotari *et al.* [7], and Diamant *et al.* [8]. Moreover, a good agreement between the experimental data and the effective $K^h\alpha_{1,2}$ linewidths indicates that the lifetimes of the K^{-2} states (about 2.2 times shorter than those of the K^{-1} states) for selected atoms with $20 \leq Z \leq 30$ are reliable. This fact enables us to reject the hypothesis reported in Ref. [8] that the large broadening of the $K^h\alpha_{1,2}$ x-ray hypersatellite lines observed in the experiment originates from a sizable (i.e., more than $\sim$2.2 times) reduction of the lifetimes of the K^{-2} states.

We believe that the results of this Letter may be helpful to better understand the relative role of the K-shell DPI mechanisms and the OIE processes leading to the complex line shapes of hypersatellite transitions decaying hollow K-shell atoms. We also hope that this work will inspire experimental research concerning the excitation photon energy dependence of the $K^h\alpha_{1,2}$ linewidths for low- and medium-Z atoms (especially in the high photon energy range).

This work was supported by the Polish Ministry of Science and Higher Education under Grant No. N N202 1465 33 and the Swiss National Science Foundation.

*mpolasik@uni.torun.pl

[1] G. Charpak, C.R. Hebd. Seances Acad. Sci. **T237**, 243 (1953).
[2] J. P. Briand *et al.*, Phys. Rev. Lett. **27**, 777 (1971).
[3] J. Hoszowska *et al.*, Phys. Rev. Lett. **102**, 073006 (2009).
[4] J. Hoszowska *et al.*, Phys. Rev. A **82**, 063408 (2010).
[5] K. Fennane *et al.*, Phys. Rev. A **79**, 032708 (2009).
[6] E. P. Kanter *et al.*, Phys. Rev. A **73**, 022708 (2006).
[7] S. Huotari *et al.*, Phys. Rev. Lett. **101**, 043001 (2008).
[8] R. Diamant *et al.*, Phys. Rev. A **79**, 062511 (2009).
[9] R. Dörner *et al.*, Radiat. Phys. Chem. **70**, 191 (2004).
[10] J. P. Mossé, P. Chevalier, and J. P. Briand, Z. Phys. A **322**, 207 (1985).
[11] J. Rzadkiewicz *et al.*, Nucl. Instrum. Methods Phys. Res., Sect. B **235**, 110 (2005).
[12] M. H. Chen, Phys. Rev. A **44**, 239 (1991).
[13] M. Polasik, Phys. Rev. A **39**, 616 (1989); **39**, 5092 (1989); **40**, 4361 (1989); **52**, 227 (1995).
[14] J. L. Campbell and T. Papp, At. Data Nucl. Data Tables **77**, 1 (2001).

[15] D. A. Papaconstantopoulos, *Handbook of Band Structure of Elemental Solids* (Plenum, New York, 1986).
[16] S. Raj *et al.*, Phys. Rev. B **65**, 193105 (2002).
[17] Th. A. Carlson *et al.*, Phys. Rev. **169**, 27 (1968).
[18] P.-A. Raboud *et al.*, Phys. Rev. A **65**, 062503 (2002).
[19] A. Knapp *et al.*, Phys. Rev. Lett. **89**, 033004 (2002).
[20] T. Schneider, P. L. Chocian, and J.-M. Rost, Phys. Rev. Lett. **89**, 073002 (2002).